Article

A High-Frequency and High-Field EPR Study of New Azide and Fluoride Mononuclear Mn(III) Complexes

Claire Mantel, Alia K. Hassan, Jacques Pcaut, Alain Deronzier, Marie-Nolle Collomb, and Carole Duboc-Toia

J. Am. Chem. Soc., **2003**, 125 (40), 12337-12344• DOI: 10.1021/ja034652+ • Publication Date (Web): 11 September 2003

J|A|C|S
ARTICLES
Published on Web 09/11/2003

A High-Frequency and High-Field EPR Study of New Azide and Fluoride Mononuclear Mn(III) Complexes

Claire Mantel,[†,§] Alia K. Hassan,[†] Jacques Pécaut,[‡] Alain Deronzier,[§] Marie-Noëlle Collomb,*[,§] and Carole Duboc-Toia*[,†]

Contribution from the Grenoble High Magnetic Field Laboratory, MPI-CNRS UPR 5021, BP 166, 38042 Grenoble Cedex 9, France, Laboratoire d'Electrochimie Organique et de Photochimie Rédox, Université Joseph Fourier, CNRS UMR 5630, Institut de Chimie Moléculaire de Grenoble (ICMG), FR CNRS 2607, and DRFMC-Service de Chimie Inorganique et Biologique, Laboratoire Coordination et Chiralité, UMR CEA-CNRS-UJF 5046, CEA-Grenoble, 38054 Grenoble Cedex, France

Received February 13, 2003; E-mail: duboc@grenoble.cnrs.fr; Marie-Noelle.Collomb@ujf-grenoble.fr

Abstract: The isolation, structural characterization and electronic properties of three new six-coordinated Mn(III) complexes, [Mn(bpea)$(F)_3$] (**1**), [Mn(bpea)$(N_3)_3$] (**2**), and [Mn(terpy)$(F)_3$] (**3**) are reported (bpea = *N,N*-bis(2-pyridylmethyl)-ethylamine; terpy = 2,2′:6′,2″-terpyridine). As for [Mn(terpy)$(N_3)_3$] (**4**) (previously described by Limburg J.; Vrettos J. S.; Crabtree R. H.; Brudvig G. W.; de Paula J. C.; Hassan A.; Barra A−L.; Duboc-Toia C.; Collomb M−N. *Inorg. Chem.* **2001**, *40*, 1698), all these complexes exhibit a Jahn−Teller distortion of the octahedron characteristic of high-spin Mn(III) ($S = 2$). The analysis of the crystallographic data shows an elongation along the tetragonal axis of the octahedron for complexes **1** and **3**, while complex **2** presents an unexpected compression. The electronic properties were investigated using a high-field and high-frequency EPR study performed between 5 and 15 K (190−575 GHz). The spin Hamiltonian parameters determined in solid state are in agreement with the geometry of the complexes observed in the crystal structures. A negative *D* value found for **1** and **3** is related to the elongated tetragonal distortion, whereas the positive *D* value determined for **2** is in accordance with a compressed octahedron. The high *E*/*D* values, in the range of 0.103 to 0.230 for all complexes, are correlated with the highly distorted geometry present around the Mn(III) ion. HF-EPR experiments were also performed on complex **1** in solution and show that the *D* value is the only spin Hamiltonian parameter which is slightly modified compared to the solid state ($D = -3.67$ cm^{-1} in solid state; $D = -3.95$ cm^{-1} in solution).

Introduction

Superoxide dismutase (SOD) is an antioxidant protein which participates in the cell's protection against formation of free radicals by dismutating the superoxide radical anion into dioxygen and hydrogen peroxide.[1] In particular, the manganese superoxide dismutase (MnSOD) is present in mitochondria and choroplasts of eukaryotes and in the cytoplasm of bacteria.[1d,2] X-ray crystal structures of MnSOD issued from both eukaryotes (human) and bacteria (*Thermus termophilus* and *Escherichia coli*) have been solved.[3] All these crystallographic data reveal a similar structure for the active site which is, in the resting state, a pentacoordinated mononuclear Mn(III) complex. During the enzymatic catalytic cycle, the oxidation level of the manganese ion switches between III and II, and electron transfer occurs. Because MnSOD is known to be among the fastest redox enzymes, structural and electronic characterization of the different reactive intermediates could not be achieved. However, during the catalytic process, the superoxide radical anion is thought to be directly coordinated to the metal center. Consistent with this view, spectroscopic studies show that small molecules such as azide and fluoride anions inhibit the enzyme by binding the manganese ion, forming stable complexes. These inhibited forms, which are believed to possess electronic structures analogous to that of the complex [MnSOD$\cdot O_2^{\bullet -}$], have been largely studied as models.[4] While a six-coordinated azide complex has been structurally characterized, no X-ray structure is available for fluoride anions, although F^- binding to Mn(III) superoxide dismutase has been demonstrated by MCD.[5]

[†] Grenoble High Magnetic Field Laboratory.
[§] Laboratoire d'Electrochimie Organique et de Photochimie Rédox.
[‡] DRFMC-Service de Chimie Inorganique et Biologique, Laboratoire Coordination et Chiralité.

(1) (a) Youn, H. D.; Kim, E. J.; Roe, J. H.; Hah, Y. C.; Kang, S. O. *Biochem. J.* **1996**, *318*, 889. (b) McCord, J. M.; Fridovich, I. *J. Biol. Chem.* **1969**, *244*, 6049. (c) Yost, F. J.; Fridovich, I. *J. Biol. Chem.* **1976**, *251*, 4905. (d) Whittaker, M. M.; Ekberg, C. A.; Edwards, R. A.; Baker, E. N.; Jameson, G. B.; Whittaker, J. W. *J. Phys. Chem. B* **1998**, *102*, 4668.
(2) Li, J.; Fisher, C. L.; Konecny, R.; Bashford, D.; Noodleman, L. *Inorg. Chem.* **1999**, *38*, 929.
(3) (a) Parker, M. W.; Blake, C. C. F. *J. Mol. Biol.* **1988**, *199*, 649. (b) Ludwig, M. L.; Metzger, A. L.; Pattridge, K. A.; Stallings, W. C. *J. Mol. Biol.* **1991**, *219*, 335. (c) Borgstahl, G. E. O.; Parge, H. E.; Hickey, M. J.; Beyer, W. F.; Hallewell, R. A.; Tainer, G. A. *Cell* **1992**, *71*, 107. (d) Wager, U. G.; Pattridge, K. A.; Ludwig, M. L.; Stallings, W. C.; Weber, M. M.; Oefner, C.; Frolow, F.; Sussman, J. L. *Protein Sci.* **1993**, *2*, 814. (e) Edwards, R. A.; Baker, H. M.; Whittaker, M. M.; Whittaker, J. W.; Jameson, G. B.; Baker E. N. *J. Biol. Inorg. Chem.* **1998**, *3*, 161.
(4) Whittaker J. W.; Whittaker, M. M. *J. Am. Chem. Soc.* **1991**, *113*, 5528.
(5) (a) Lah, M. S.; Dixon, M. M.; Pattridge, K. A.; Stallings, W. C.; Fee, J. A.; Ludwig, M. L. *Biochemistry* **1995**, *34*, 1646−1660. (b) Whittaker, M. M.; Whittaker, J. W. *Biochemistry* **1996**, *35*, 6762.

Concerning synthetic complexes, only few crystallographically characterized mononuclear Mn(III) azide[6,7] and fluoride[8] complexes have been published. In this context, the synthesis of new Mn(III) model complexes, in addition to a complete characterization of their physical properties, seems to be necessary.

In this article, we focus our attention on the study of a series of new six-coordinated mononuclear Mn(III) compounds synthesized in the presence of azide or fluoride anions. The complexes $[Mn^{III}(bpea)(F)_3]$ (**1**) (bpea = *N*,*N*-bis(2-pyridylmethyl)-ethylamine), $[Mn^{III}(bpea)(N_3)_3]$ (**2**), and $[Mn^{III}(terpy)(F)_3]$ (**3**) (terpy = 2,2′:6′,2″-terpyridine) have been isolated and structurally characterized. The aim of our work was also to determine precisely the electronic properties of this series of compounds to correlate them with their structural properties. Because in these systems Mn(III) is a high-spin d^4 Jahn−Teller ion with an integer spin ground state ($S = 2$), their electronic structure determination cannot be achieved by X-band EPR. The high-field and high-frequency EPR technique (HF-EPR) has been already applied with success for the analysis of $[Mn(terpy)(N_3)_3]$ (**4**), the first complex of our series.[7] In that case, a multifrequency EPR study was done and allowed us to determine precisely the spin Hamiltonian parameters issued from eq 1.

$$H = \beta B\mathbf{g}S + D[S_z^2 - (1/3)S(S+1)] + E(S_x^2 - S_y^2) \quad (1)$$

This analysis revealed a large E/D ratio of 0.15 in accordance with the highly distorted octahedron geometry adopted around the Mn ion. This complex was the first mononuclear Mn(III) complex with such rhombicity studied by HF-EPR spectroscopy. All the others mononuclear Mn(III) complexes that have been studied by this technique are axial or nearly axial.[9]

We describe in this paper the precise determination of the spin Hamiltonian parameters of complexes **1**, **2**, and **3** which was performed by a multifrequency EPR study. Their rhombic symmetry allows us to discuss the magnitude of the *D* and *E* terms as a function of the degree of distortion of the different complexes. We also report HF-EPR spectra of complex **1** obtained in solution.

Experimental Section

Manganese fluoride ($[Mn^{III}(F)_3]$), manganese acetate ($[Mn^{III}(OAc)_3]\cdot 2H_2O$), and sodium azide ($NaN_3$) were purchased from Aldrich and used without further purification.

Ligands and Complexes. The ligand 2,2′:6′,2″-terpyridine (terpy) was purchased from Aldrich. The ligand *N*,*N*-bis(2-pyridylmethyl) ethylamine (bpea) was synthesized according to a method described previously.[10]

Synthesis of $[Mn^{III}(bpea)(F)_3]$ (Complex 1). To a stirred solution of bpea (33 mg, 0.145 mmol) in 3 mL of methanol was added $[Mn^{III}(F)_3]$ (15.9 mg, 0.145 mmol). The resulting brown solution was stirred at room temperature for 1 h, filtered to eliminate the impurities, and evaporated to dryness. The resulting red powder corresponding to complex **1** was obtained. Single crystals of $[Mn^{III}(bpea)(F)_3]\cdot H_2O$ were grown by slow diffusion of diethyl ether in a concentrated solution of **1** in acetonitrile (CH_3CN) (17.9 mg, yield, 36.4%). These crystals conformed well to the stoichiometry $[Mn^{III}(bpea)(F)_3]\cdot 1.5H_2O$. Elemental anal. calcd for complex $\mathbf{1}\cdot 1.5H_2O$ ($MnF_3N_3H_{20}C_{14}O_{1.5}$): C, 46.02; N, 11.51; H, 5.52. Found: C, 45.83; N, 11.40; H, 5.33. IR in cm^{-1} (KBr): ν = 3450 (vs, br), 2925 (w, br), 1651 (m), 1605 (s), 1574 (m), 1556 (w), 1538 (w), 1480 (m), 1446 (m), 1392 (m), 1359 (w), 1314 (w), 1291 (w), 1156 (w), 1104 (w), 1049 (w), 1019 (w), 1001 (w), 860 (w), 803 (m), 773 (s), 729 (w), 596 (vs, br), 416 (w). Electronic spectral data in CH_3CN solution (λ_{max} in nm (ϵ in M^{-1} cm^{-1})): 204 (sh, 12400), 258 (6100), 443 (298), 520 (124), 734 (88).

Synthesis of $[Mn^{III}(bpea)(N_3)_3]$ (Complex 2). To a stirred solution of $[Mn^{III}(OAc)_3]\cdot 2H_2O$ (70.8 mg, 0.263 mmol) in 4 mL of methanol was added bpea (59.7 mg, 0.263 mmol). The addition of an excess of solid NaN_3 precipitated the complex **2** as a black microcrystalline product, which was then filtered and dried under reduced pressure (58.6 mg, yield 54.6%). This product conformed well to the stoichiometry $[Mn^{III}(bpea)(N_3)_3]\cdot CH_3OH$. Elemental anal. calcd for $\mathbf{2}\cdot CH_3OH$ ($MnN_{12}H_{21}C_{15}O_1$): C, 40.91; N, 38.17; H, 4.81. Found: C, 40.41; N, 38.20; H, 4.10. IR in cm^{-1} (KBr): ν = 3428 (vs, br), 2924 (vs, br), 2044 (vs), 2069 (vs), 1603 (s), 1573 (w), 1556 (w), 1485 (m), 1444 (s), 1385 (w), 1355 (w), 1329 (s), 1287 (m), 1157 (w), 1106 (w), 1034 (w), 1021 (m), 992 (w), 971 (w), 953 (w), 855 (w), 804 (m), 765 (s), 725 (w), 646 (m), 591 (w), 538 (w), 509 (w), 477 (w), 448 (s), 382 (w), 351 (w). Electronic spectral data in CH_3CN solution (λ_{max} in nm (ϵ in M^{-1} cm^{-1})): 197 (37 070), 248 (11 700), 334 (7800), 446 (4400). Single crystals of $[Mn^{III}(bpea)(N_3)_3]$ were grown by slow evaporation of a solution of complex **2** in dichloromethane (CH_2Cl_2). During the crystallization, some colorless crystals of the binuclear complex $[Mn_2^{II,II}(\mu\text{-}N_3)(bpea)_2(N_3)_2]$ were also formed.[11] For this reason, all spectroscopic analysis was performed on the microcrystalline product which is contaminated by less than 5% of the binuclear complex. CAUTION: both N_3^- and its complexes are potentially explosive. Although we have encountered no such problems with complex **2**, it should still be handled with care. Further, N_3^- releases explosive HN_3 on contact with acid solution.

Synthesis of $[Mn^{III}(terpy)(F)_3]$ (Complex 3). To a stirred solution of terpy (50 mg, 0.214 mmol) in 3 mL of methanol was added $[Mn^{III}(F)_3]$ (23.95 mg, 0.214 mmol). The resulting brown solution was stirred at room temperature for 2 h and then filtered to eliminate the impurities. Slow diffusion of diethyl ether in this solution afforded red crystals of $[Mn^{III}(terpy)(F)_3]\cdot CH_3OH\cdot 1/3H_2O$ (112.5 mg, yield 76%). These crystals conformed well to the stoichiometry $[Mn^{III}(terpy)(F)_3]\cdot 2.5H_2O$. Elemental anal. calcd for $\mathbf{3}\cdot 2.5H_2O$ ($MnF_3N_3H_{16}C_{15}O_{2.5}$): C, 46.15; N, 10.77; H, 4.13. Found: C, 46.01; N, 10.57; H, 4.17. IR in cm^{-1} (KBr): ν = 3445 (vs, br), 3082 (w, br), 1634 (w), 1596 (s), 1576 (m), 1498 (w), 1479 (m), 1453 (s), 1404 (w), 1312 (m), 1248 (m), 1197 (w), 1165 (m), 1097 (w), 1018 (m), 776 (s), 740 (w), 667 (w), 651 (w), 641 (w), 597 (vs, br). Electronic spectral data in methanol solution (λ_{max} in nm (ϵ in M^{-1} cm^{-1})): 207 (sh, 28 830), 234 (19 240), 275 (19 430), 327 (10 430), 430 (sh, 38), 460 (62), 480 (68), 720 (11).

Physical Measurements. UV/vis spectra were recorded on a Cary 1 Varian spectrophotometer. IR spectra were obtained with Perkin-Elmer Spectrum GX spectrophotometer, piloted by a Dell Optiplex GXa computer. Spectra were recorded with a solid sample at 1% in mass in a pellet of KBr. High-frequency and high-field EPR spectra were

(6) (a) Wieghardt, K.; Bossek, U.; Nuber, B.; Weiss, J. *J. Inorg. Chim. Acta* **1987**, *126*, 39. (b) Meyer, K.; Bendix, J.; Metzler-Nolte, N.; Weyhermüller, T.; Wieghardt, K. *J. Am. Chem. Soc.* **1998**, *120*, 7260.
(7) Limburg, J.; Vrettos, J. S.; Crabtree, R. H.; Brudvig, G. W.; de Paula, J. C.; Hassan, A.; Barra, A.-L.; Duboc-Toia, C.; Collomb, M.-N. *Inorg. Chem.* **2001**, *40*, 1698.
(8) Numez, P.; Elias, C.; Fuentes, J.; Solans, X.; Tressaud, A.; Marco de Lucas, M. C.; Rodriguez, F. *J. Chem. Soc., Dalton Trans.* **1997**, 4335.
(9) (a) Goldberg, D. P.; Telser, J.; Krzystek, J.; Montalban, A. G.; Brunel, L. C.; Barrett, A. G. M.; Hoffman, B. M. *J. Am. Chem. Soc.* **1997**, *119*, 8722. (b) Krzystek, J.; Telser, J.; Pardi, L.-A.; Goldberg, D.-P.; Hoffman, B.-M.; Brunel, L.-C. *Inorg. Chem.* **1999**, *38*, 6121. (c) Bendix, J.; Gray, H. B.; Golubkov, G.; Gross, Z. *J. Chem. Soc., Chem. Commun.* **2000**, 1957. (d) Barra, A.-L.; Gatteschi, D.; Sessoli, R.; Abatti, G.-L.; Cornia, A.; Fabretti, A.-C.; Uytterhoeven, M.-G. *Angew. Chem., Int. Ed. Engl.* **1997**, *36*, 2329. (e) Mossin, S.; Weihe, H.; Barra, A.-L. *J. Am. Chem. Soc.* **2002**, *124*, 8764.
(10) Pal, S.; Chan, M. K.; Armstrong, W. H. *J. Am. Chem. Soc.* **1992**, *114*, 6398−6406.
(11) Mantel, C.; Pécaut, J.; Deronzier, A.; Duboc, C.; Collomb, M.-N. Manuscript in preparation.

Table 1. Principal Crystallographic Data and Parameters of Complexes $[Mn(bpea)(F)_3]$ (**1**), $[Mn(bpea)(N_3)_3]$ (**2**), and $[Mn(terpy)(F)_3]$ (**3**)

compound	**1**·H_2O	**2**	**3**·CH_3OH·1/3H_2O
chemical formula	$C_{14}H_{19}F_3MnN_3O$	$C_{14}H_{17}MnN_{12}$	$C_{16}H_{15,60}F_3MnN_3O_{1,30}$
formula weight	357.26	408.34	382.67
temperature (K)	223	223	193
wavelength (Å)	0.71073	0.71073	0.71073
crystal system	triclinic	orthorhombic	monoclinic
space group	$P\bar{1}$	*Pbca*	*P*2(1)/*c*
a (Å)	8.7050(15)	8.5919(6)	10.0235(8)
b (Å)	13.351(2)	15.7208(11)	9.8795(8)
c (Å)	13.484(2)	27.2838(19)	16.5225(13)
α (deg)	87.207(3)	90	90
β (deg)	84.974(3)	90	101.181(2)
γ (deg)	81.127(3)	90	90
volume ($Å^3$), *Z*	1541.4(5), 4	3685.3(4), 8	1605.1(2), 4
density (mg/m^3)	1.540	1.472	1.584
μ (mm^{-1})	0.892	0.744	0.865
R1, wR2[a]	0.0500, 0.1004	0.0603, 0.0691	0,0819, 0.1124

[a] $R1 = \sum||F_o| - |F_c||/\sum|F_o|$, $wR2 = [(\sum w(|F_o| - |F_c|)^2/\sum wF_o^2)]^{1/2}$.

Table 2. Selected Bond Distances (Å) for Complexes **1**, **2**, and **3**

compound	**1**·H_2O	**2**	**3**·CH_3OH·1/3H_2O
Mn−N(1)	2.1883(17)	2.2905(12)	2.0952(8)
Mn−N(2)	2.2673(18)	2.1808(13)	2.2561(9)
Mn−N(3)	2.2566(18)	2.1832(14)	2.2370(9)
Mn−F(1)	1.8191(13)		1.8342(6)
Mn−N(4)		2.0025(14)	
Mn−F(2)	1.8355(12)		1.8137(7)
Mn−N(5)		1.9695(15)	
Mn−F(3)	1.8191(12)		1.8511(6)
Mn−N(6)		1.9609(15)	

recorded on a laboratory-made spectrometer[12] using powder samples pressed in pellets to avoid preferential orientation of the crystallites in the strong magnetic field. Gunn diodes operating at 95 and 115 GHz and equipped with a second-, third-, fourth-, and fifth-harmonic generators have been used as a radiation source. The magnetic field was produced by a superconducting magnet (0−12 T) or a resistive magnet (0−20 T).

Crystal Structure Determination of Complexes 1·H_2O, 2 and 3·CH_3OH·1/3H_2O. A crystal of complex **1** of dimensions 0.2 × 0.2 × 0.4 mm^3 was selected. For complexes **2** and **3**, the dimensions are similar to the ones measured for complex **1**. Diffraction data were collected on Brucker SMART diffractometer with Mo Kα radiation. The crystallographic data are summarized in Tables 1, 2, and 3. All calculations were effected using the SHELTL computer program.[13] The full details of the X-ray structure determination can be found in the Supporting Information.

Results

Crystal Structure Determination. The crystal structures of $[Mn^{III}(bpea)(F)_3]\cdot H_2O$ (**1**·H_2O), $[Mn^{III}(bpea)(N_3)_3]$ (**2**), and $[Mn^{III}(terpy)(F)_3]\cdot CH_3OH\cdot 1/3H_2O$ (**3**·CH_3OH·1/3H_2O) have been determined by single-crystal X-ray crystallography. Table 1 gives the principal crystallographic data of complexes **1**, **2**, and **3**, while Tables 2 and 3 summarize selected bond distances and angles. Figure 1 displays their structures.

A common feature of these structures is the geometry adopted around the Mn(III) ion which is in the center of a highly distorted octahedron. In the three complexes, Mn(III) is a high-spin ion d^4 with an integer spin ground state $S = 2$. For high-spin Mn(III) systems, the Mn−N bond lengths are generally equal to or longer than 2 Å, whereas in low-spin Mn(III) systems ($S = 1$) the Mn−N bond lengths never exceed 2 Å.[14] For complexes **1**, **2**, and **3**, the lengths of the $Mn-N_{(bpea\ or\ terpy)}$ are longer than 2 Å (Table 2). Therefore, a tetragonal distortion of the octahedron is awaited as signature of Jahn−Teller effect characteristic of high-spin Mn(III) ion.

Table 3. Selected Bond Angles (deg) for Complexes **1**, **2**, and **3**

compound	**1**·H_2O	**2**	**3**·CH_3OH·1/3H_2O
F(3)−Mn−F(1)	90.02(6)		91.33(3)
N(5)−Mn−N(6)		88.40(6)	
F(3)−Mn−F(2)	179.51(6)		175.34(3)
N(5)−Mn−N(6)		177.22(6)	
F(1)−Mn−F(2)	90.46(6)		93.20(3)
N(4)−Mn−N(6)		92.28(6)	
F(3)−Mn−N(1)	94.30(6)		87.24(3)
N(5)−Mn−N(1)		92.61(5)	
F(1)−Mn−N(1)	175.63(6)		175.53(3)
N(4)−Mn−N(1)		175.02(6)	
F(2)−Mn−N(1)	85.22(6)		88.32(3)
N(6)−Mn−N(1)		86.93(5)	
F(3)−Mn−N(3)	89.37(6)		87.21(3)
N(5)−Mn−N(3)		92.35(6)	
F(1)−Mn−N(3)	104.36(7)		109.31(3)
N(4)−Mn−N(3)		99.76(6)	
F(2)−Mn−N(3)	90.58(6)		90.27(3)
N(6)−Mn−N(3)		90.19(6)	
N(1)−Mn−N(3)	75.06(6)	75.33(5)	74.87(3)
F(3)−Mn−N(2)	87.69(6)		89.61(3)
N(5)−Mn−N(2)		89.04(6)	
F(1)−Mn−N(2)	106.36(7)		101.07(3)
N(4)−Mn−N(2)		109.11(6)	
F(2)−Mn−N(2)	92.10(6)		90.59(3)
N(6)−Mn−N(2)		88.19(6)	
N(1)−Mn−N(2)	74.53(6)	75.79(5)	74.69(3)
N(3)−Mn−N(2)	149.13(6)	151.12(5)	149.51(3)

Table 4. Electronic and Structural Parameters for Complexes **1**, **2**, **3**, and **4**

compound	**1**	**2**	**3**	**4**
D (cm^{-1})	−3.67(2)	+3.50(1)	−3.82(2)	−3.29(1)
E (cm^{-1})	0.70(2)	0.82(1)	0.75(2)	0.48(1)
g_x	1.96(1)	2.02(1)	1.97(2)	2.00(0.5)
g_y	1.98(1)	1.98(1)	2.04(1)	1.98(0.5)
g_z	1.98(1)	1.95(1)	1.96(1)	2.01(0.5)
E/*D*	−0.191	0.230	−0.109	−0.146
bond distances (Å)[a]	4.007	4.293	3.929	4.068
	3.655	**3.930**	3.665	3.952
	4.524	4.364	**4.493**	**4.492**
tetragonal distortion	elongation	compression	elongation	elongation

[a] Addition of the two bond distances along the three axes of the octahedron: Mn−N(1) + (Mn−F(1) or Mn−N(4)); (Mn−F(2) + Mn−F(3)) or (Mn−N(5) + Mn−N(6)); Mn−N(2) + Mn−N(3).

In complexes **1** and **3**, a tetragonal elongation along the N(2)−N(3) axis is observed (Tables 2 and 4). Consequently, the equatorial plane is defined by the three anions F^- and the central nitrogen of bpea (**1**) or terpy (**3**). This plane is similar to the one proposed for the complex $[Mn^{III}(terpy)(N_3)_3]$ (**4**), previously described, which also presents a tetragonal elongation.[7] The axial positions are occupied by the two aromatic nitrogen atoms N(2) and N(3) of the bpea (**1**) or terpy (**3**) ligand. It should be noticed that in **1**, the bpea ligand adopts an uncommon meridional mode coordination around the Mn(III) ion.

(12) (a) Barra, A.-L.; Brunel, L.-C.; Robert, J.-B. *Chem. Phys. Lett.* **1990**, *165*, 107. (b) Muller, F.; Hopkins, M.-A.; Coron, N.; Grynderg, M.; Brunel, L.-C.; Martinez, G. *Rev. Sci. Instrum.* **1989**, *60*, 3681.
(13) Sheldric, G. M. *SHELXTL-Plus*, version 5.1; Structure Determination Software Programs; Bruker-AXS Inc.: Madison, WI, 1998.
(14) Ganguly, S.; Karmakar, S.; Chakravorty, A. *Inorg. Chem.* **1997**, *36*, 116.

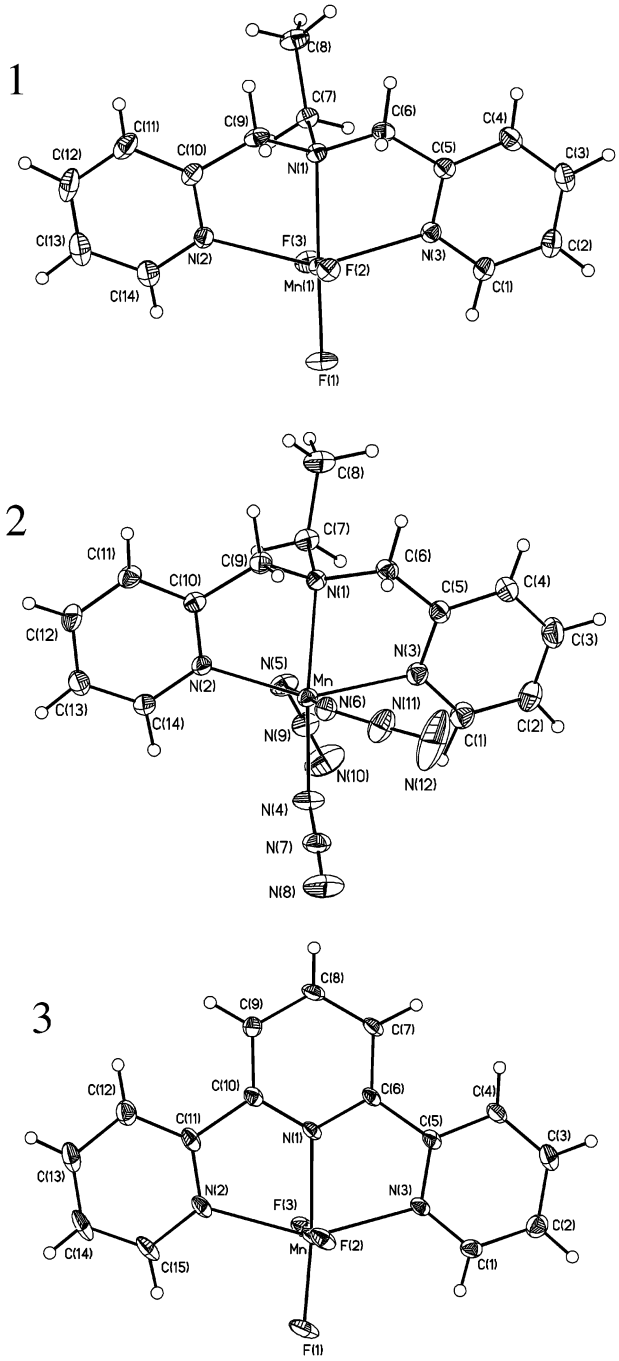

Figure 1. ORTEP diagrams showing the molecular structure of complexes **1**, **2**, and **3**. Hydrogen atoms have been omitted for clarity.

The tridentate ligands, bpea, or terpy induce similar tetragonal distortions: (i) the elongation is comparable for both complexes: for **1**, Mn−N(2), 2.2673(18) Å; Mn−N(3), 2.2566(18) Å and for **3**, Mn−N(2), 2.2561(9) Å; Mn−N(3), 2.2370(9) Å; (ii) for **1** and **3**, the N(2)−Mn−N(3) angle is respectively equal to 149.13(6)° and 149.51(3)° compared to 180°, the theoretical value (Table 3).

The equatorial plane distortion is due to the presence of the central nitrogen atom N(1) of bpea or terpy, which forms longer bonds with the Mn ion than with the fluoride atom. Moreover, in that case, the nature of the tridentate ligand affects the deformation. The bpea ligand induces a larger one compared to terpy, because the Mn−N(1) bond is longer in **1** (Mn−N(1), 2.1883(17) Å) than in **3** (Mn−N(1), 2.0952(8) Å) and the Mn−F bonds are shorter than the Mn−N bonds. All of the Mn−F bond lengths are between 1.814 and 1.851 Å and are in the range expected for such bonds.[8]

Controversially, we propose to describe complex **2** as a compressed octahedron in a very highly distorted geometry. The tetragonal compression occurs along the N(5)−N(6) axis (Tables 2 and 4), and the equatorial plane is defined by the three nitrogen atoms of bpea and the nitrogen atom of one azide anion, N(4). In this structure, the bpea ligand is also coordinated to the Mn(III) ion in a meridional mode. Even if the octahedron is defined by a different tetragonal axis in the two azide complexes (**2** and **4**), the Mn−N(5) and Mn−N(6) bond distances are similar (for **2**, Mn−N(5), 1.9695(15) Å; Mn−N(6), 1.9609(15) Å and for **4**, Mn−N(5), 1.987(2) Å; Mn−N(6), 1.965(2) Å). On the other hand, the Mn−N(2), Mn−N(3) bond distances respectively equal to 2.1808(13) Å and 2.1832(14) Å in **2** are shorter than those in **4** (Mn−N(2), 2.234(2) Å; Mn−N(3), 2.258-(2) Å). The equatorial plane bears an important deformation in **2** with the N(2)−Mn−N(3) angle of 151.12(5)° compared to the expected value of 180° (Table 3). The $Mn-N_{azide}$ distances for **2** (average, 1.9776(0.0220) Å) are similar to the ones observed for **4**, (average, 1.970(0.015) Å) but shorter than those for $[Mn(tacn)(N_3)_3]$[6a] (average, 2.011(0.139) Å) and $[Mn(cyclam)(N_3)_2](ClO_4)$[6b] (average, 2.171(0.006) Å).

Multifrequency EPR Study. The high-field and high-frequency experiments were performed on polycrystalline powder pellets to avoid magnetic orientation of crystals. A multi-frequency EPR study between 190 and 575 GHz was accomplished over a temperature range of 5−15 K.

Complex 1. Figure 2 shows experimental and simulated HF-EPR spectra recorded at 15 K and at 475 GHz. In Figure 3, the effect of the temperature on the spectra recorded at 475 GHz is shown.

In the low-field part of the experimental spectrum 2D, "forbidden" transitions are observed. Thus, the character of a transition can be determined by the value of the slope of the line ($\rho = h/g\beta$) which is directly related to the g value of the observed transition. An "allowed" transition has a g value close to the one expected for the studied metallic ion. For a Mn(III) ion, a value close to $g = 2$ is expected. On the other hand, "forbidden" transitions are characterized by high g values larger than $g = 2$. Other characteristics of these last transitions are: (i) their intensity is enhanced as the EPR frequency decreases and (ii) they are located in the low field part of the spectra where strong-field limit conditions are not reached ($D \gg g\beta B$).

The transition seen at 5.49 T at 475 GHz (Figure 2B) has been attributed to the first transition of the quintuplet associated to the z axis. This axis attribution was based on the fact that this transition is the one located further from the center of the spectrum (close to $g = 2$ for a Mn(III) ion). Then, an evaluation of the D value can be made from its field position because the energy gap between this transition and the center of the spectrum corresponds to $3|D|$. At 475 GHz, the $g = 2$ value is located at 16.96 T, which gives a field difference of 11.47 T, corresponding to a D value of 3.82 cm^{-1} for complex **1**. Because it was already mentioned in previous papers, the sign of the D parameter can be determined by simple observation of high-frequency and low-temperature EPR spectra.[15] Under these conditions, the lowest energy levels of the $S = 2$ multiplet are populated and the

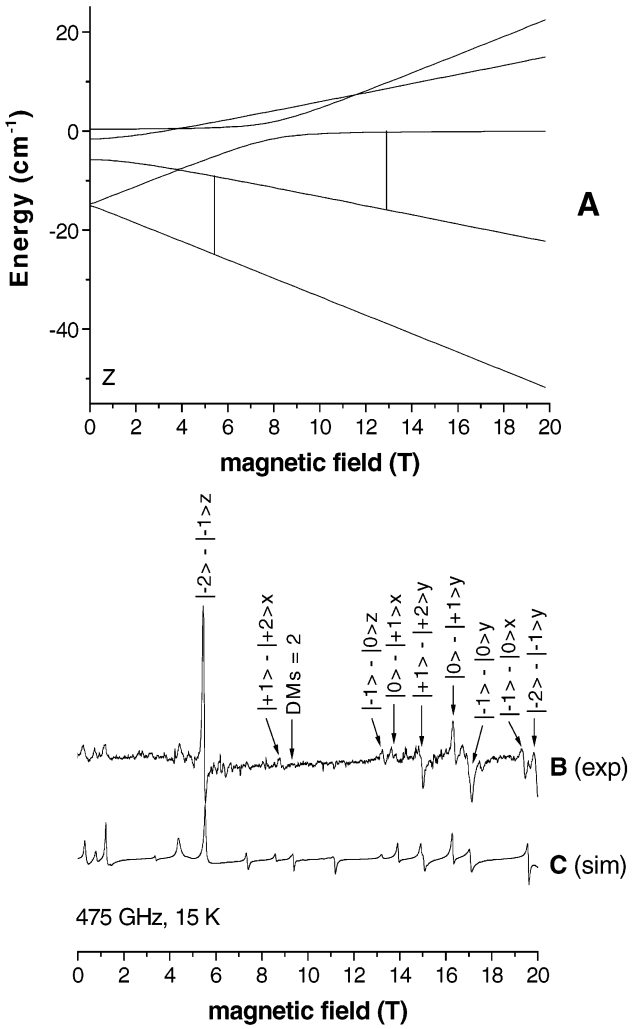

Figure 2. Plots of energy vs field for the five levels arising from an $S = 2$ spin state using parameters written below. The field is parallel to the molecular axis, along z (A). The observed resonances at 475 GHz are indicated by vertical bars. Experimental (B) and simulated (C) powder HF-EPR spectra of complex **1** recorded at 475 GHz and at 15 K. The parameters used for the simulations are $D = -3.67(2)$ cm^{-1}, $E = 0.70(2)$ cm^{-1}, $g_x = 1.96(1)$, $g_y = 1.98(1)$, and $g_z = 1.98(1)$.

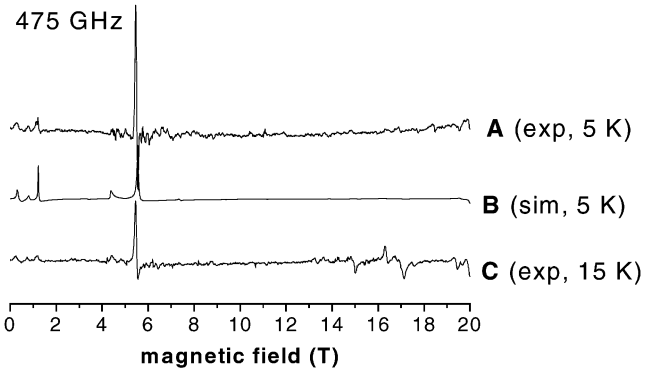

Figure 3. Experimental (A and C) and simulated (B) powder HF-EPR spectra of complex **1** recorded at 475 GHz and at two different temperatures: 5 K (A and B) and 15 K (C).

transitions associated to the z axis are located in the high-field part of the spectrum for $D > 0$, while the opposite is true for

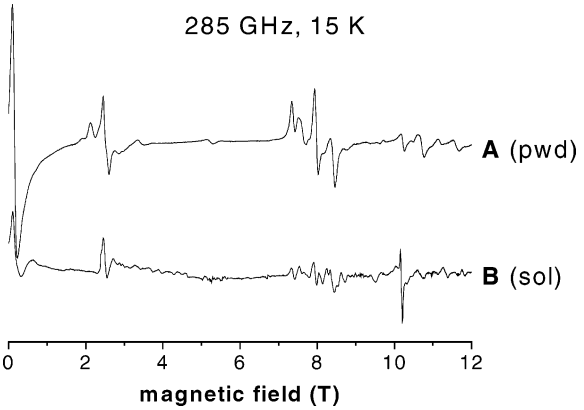

Figure 4. Experimental powder (A) and solution (B) HF-EPR spectra of complex **1** recorded at 285 GHz and at 15 K.

$D < 0$. At 5 K and 475 GHz (Figure 3A), the $|2, -2\rangle \rightarrow |2, -1\rangle$ transition along the z axis located in the low-field part of the spectrum is, then, the signature of a negative D value for complex **1**.

The HF-EPR spectra were simulated using a full-matrix diagonalization procedure of the Hamiltonian (eq 1) for the $S = 2$ ground spin state.[16] Simulated spectra (Figures 2C and 3B) are reported at 475 GHz. The spin Hamiltonian parameters used for these simulations are: $D = -3.67(2)$ cm^{-1}, $E = 0.70(2)$ cm^{-1}, $g_x = 1.96(1)$, $g_y = 1.98(1)$, and $g_z = 1.98(1)$ (Table 4). The simulations reproduce with a good agreement the intensity, the position, and the shape of the "allowed" features, as well as those of the "forbidden" transitions present in the experimental spectra. The D and g values determined by simulation are close to the values calculated above and are acceptable for all frequencies and temperatures.

At this point, the attribution of the different transitions becomes feasible. The two first transitions of the $S = 2$ multiplet along the z axis can be attributed with the spectrum recorded at 475 GHz (Figure 2A and 2B). The $|2, -1\rangle \rightarrow |2, 0\rangle$ transition can be observed only at 15 K because at 5 K, the energy level $M_S = -1$ is not populated (Figure 3A). Along the x and y axes, the E value affects the energy levels and complicates the diagram. Along the x direction, the first transition of the $S = 2$ multiplet cannot be observed at 475 GHz in this field range. The three other transitions are located at 19.6, 13.9, and 8.6 T (Figure 2B). Along the y direction, the four expected transitions are observed, and their attribution is given in Figure 2.

We also performed a multi-frequency EPR analysis of **1** in acetonitrile at 5 and 15 K. Figure 4B shows the experimental spectrum recorded at 285 GHz and at 15 K. At $g = 2$, a new signal appears which is probably due to the decomposition of a small amount of **1** into Mn(II) (less than 2%). The presence of Mn(II) in very low concentration in the mononuclear Mn(III) sample is rather usual and was already observed in different HF-EPR studies on Mn(III) systems.[7,17] Otherwise, the spectrum shown in Figure 4B is comparable to that obtained from the powder (Figure 4A). The slight differences correspond mainly to small shifts. The parameters are $D = -3.95(8)$ cm^{-1}, $E = 0.70(2)$ cm^{-1}, $g_x = 1.96(1)$, $g_y = 1.98(1)$, and $g_z = 1.98(1)$, similar to the ones measured for **1** in solid state, except for the

(15) (a) Telser, J.; Pardi, L. A.; Krzystek, J.; Brunel, L.-C. *Inorg. Chem.* **1998**, *37*, 5769. (b) Barra, A.-L.; Gatteschi, D.; Sessoli, R. *Chem.—Eur. J.* **2000**, *6*, 1608.

(16) Jacobsen, C. J. H.; Pedersen, E.; Villardsen, J.; Weihe, H. *Inorg. Chem.* **1993**, *32*, 1216.

(17) Krzystek, J.; Telser, J.; Hoffman, B. M.; Brunel, L.-C.; Licoccia, S. *J. Am. Chem. Soc.* **2001**, *123*, 7890.

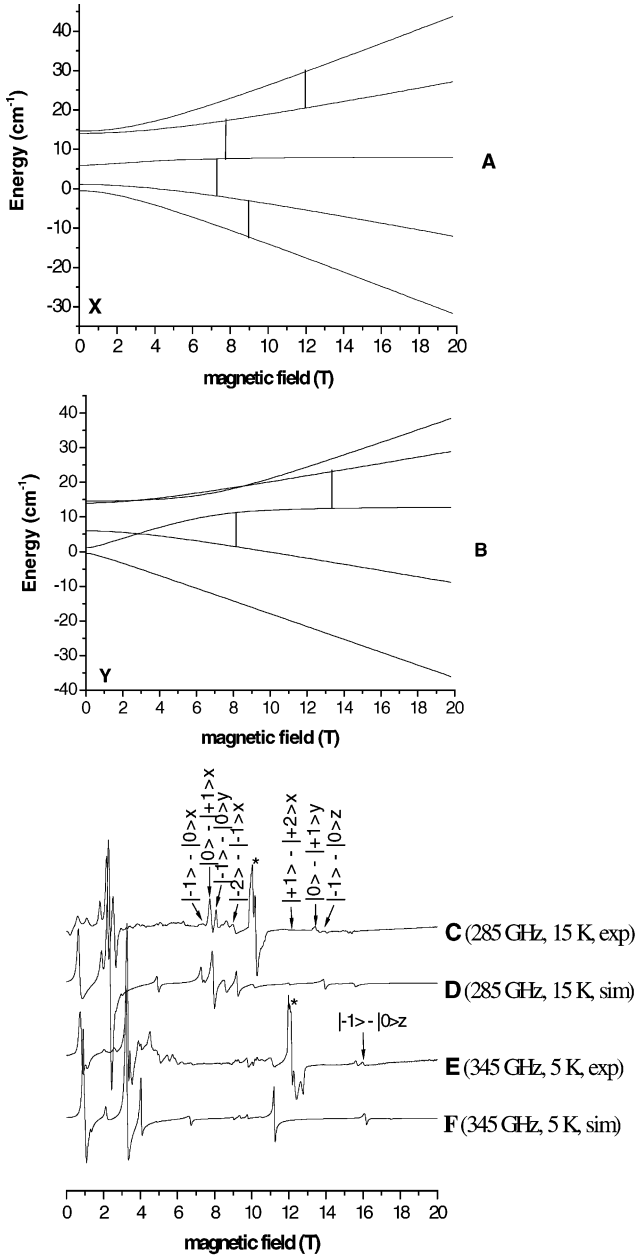

Figure 5. Plots of energy vs field for the five levels arising from an $S = 2$ spin state using parameters written below. The field is parallel to the molecular axis, along x (A) and y (B). The observed resonances at 285 GHz are indicated by vertical bars. Experimental (at 285 GHz (C) and at 345 GHz (E)) and simulated (at 285 GHz (D) and at 345 GHz (F)) powder HF-EPR spectra of complex **2** recorded at 15 K (C and D) and 5 K (E and F). The parameters used for the simulations are $D = +3.50(1)$ cm^{-1}, $E = 0.82(1)$ cm^{-1}, $g_x = 2.02(1)$, $g_y = 1.98(1)$, and $g_z = 1.95(1)$. The transitions located at $g = 2$ and marked with an asterisk (*) in the experimental spectra originate from an impurity $[Mn_2^{II,II}(\mu\text{-}N_3)(bpea)_2(N_3)_2]$ (see in the Experimental Section).

D term which is slightly higher ($D = -3.67(2)$ cm^{-1} in solid state). The obtained spin Hamiltonian parameters successfully simulate likewise HF-EPR spectra recorded at all temperatures and frequencies.

Complex 2. The same EPR analysis was performed for complex **2**. Figure 5 displays simulated and experimental HF-EPR spectra recorded at two different frequencies (285 and 345 GHz). A signal, which is not related to complex **2**, is present at $g = 2$. This impurity was unambiguously identified as a binuclear Mn(II) complex: $[Mn_2^{II,II}(\mu\text{-}N_3)(bpea)_2(N_3)_2]$ (see

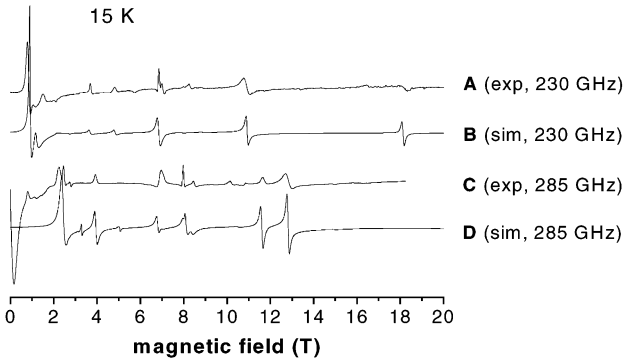

Figure 6. Experimental (at 230 GHz (A) and at 285 GHz (C)) and simulated (at 230 GHz (B) and at 285 GHz (D)) powder HF-EPR spectra of complex **3** recorded at 5 K. The parameters used for the simulation are $D = -3.82(2)$ cm^{-1}, $E = 0.75(2)$ cm^{-1}, $g_x = 1.97(2)$, $g_y = 2.04(1)$, $g_z = 1.96(1)$.

Experimental Section). A set of spin Hamiltonian parameters was determined for complex **2**: $D = +3.50(1)$ cm^{-1}, $E = 0.82(1)$ cm^{-1}, $g_x = 2.02(1)$, $g_y = 1.98(1)$, and $g_z = 1.95(1)$ (Table 4). This set allowed us to simulate the spectra recorded at all frequencies and temperatures.

Since the D value is positive, the first transitions of the $S = 2$ multiplet associated with the z axis are located in the high-field part of the spectra. Even with a field up to 20.0 T, the $|2, -2\rangle \rightarrow |2, -1\rangle$ transition cannot be observed along the z axis, whereas the $|2, -1\rangle \rightarrow |2, 0\rangle$ transition is located at 16.05 T at 345 GHz (Figure 5E). The energy difference between this transition and the center of the spectrum corresponds to $|D|$ and is equal to 3.74 T (3.52 cm^{-1}), in agreement with the value given above. The attribution and characterization of the other transitions have been performed thanks to the multifrequency and variable-temperature EPR study (Figure 5).

Complex 3. Experimental and simulated HF-EPR spectra recorded at 15 K and at 230 and 285 GHz are given in the Figure 6. The spin Hamiltonian parameters are: $D = -3.82(2)$ cm^{-1}, $E = 0.75(2)$ cm^{-1}, $g_x = 1.97(2)$, $g_y = 2.04(1)$, and $g_z = 1.96(1)$ (Table 4). As with complexes **1** and **4**, complex **3** presents a negative D with a comparable magnitude, while the E/D value of -0.109 is the weakest.

Discussion

In this paper, we described the synthesis and the crystallographic characterization of a series of new mononuclear Mn(III) complexes possessing a fluoride or azide anion and a tridentate ligand bpea or terpy. The Mn−F bond distances are shorter than the Mn−N_{azide} ones, in accordance with the greater electronegativity of a fluoride anion compared to that of an azide anion. The four complexes present a similar geometry, resulting in a meridional coordination mode of the tridentate ligand bpea and terpy. Thus, this series is perfectly adapted to enable us to understand the effect of small structural modifications around the Mn(III) ion on the electronic properties of the complexes.

As a result of the tetragonal Jahn−Teller deformation, the observation of a compression in the octahedron in **2** was unexpected, compared to an elongation in complexes **1**, **3**, and **4**. The observed compression along the tetragonal N(5)−N(6) axis in **2** is due to the fact that the Mn−N(2) and Mn−N(3) bonds are shortened compared to those in the other complexes (Tables 2 and 4). To explain the difference between the two bpea complexes, **1** and **2**, our hypothesis is based on the

electron-donating character of each anion. In **1**, the short Mn−F bonds induce longer Mn−N(2) and Mn−N(3) bonds. If we compare the azide complexes, **2** and **4**, the nature of the bpea ligand, which is less rigid than the terpy ligand, permits the compression of the Mn−N(2) and Mn−N(3) bonds in **2**.

These structural observations are confirmed by the multifrequency EPR study. The negative *D* values found for complexes **1**, **3**, and **4** are in agreement with an elongated octahedral structure around the Mn(III) ion, whereas the positive *D* value observed for complex **2** is in accordance with a compressed octahedron. Predictions of the *D* sign originate from the classical ligand field theory.[18] Nevertheless, it has been recently shown that the valence bond configuration interaction has to be taken into account as a contribution to *D* if the UV−visible spectrum of a Mn(III) complex is characterized by a low-energy ligand-to-metal charge transfer (LMCT) transition.[9e] Depending on the magnitude of this positive contribution, the *D* sign can be inverted for an elongated Mn(III) octahedron. The optical properties of our complexes indicate the absence of low-energy LMCT transition, allowing us to describe our system only by a classical ligand field theory. It should be noticed that tetragonal compressions are uncommonly observed for octahedral Mn(III) systems.[19] Moreover, it is the first time that a compressed octahedral mononuclear complex was studied by EPR, and therefore the sign of *D* was unambiguously determined for that kind of octahedral geometry.

In the following discussion, the electronic and structural properties of complexes **1**, **3**, and **4** are compared. The geometry around the Mn(III) ion corresponds to a highly distorted octahedron due to several deformations observed in the structure: (i) the elongation along the N(2)−N(3) axis as the result of the tetragonal distortion due to the Jahn−Teller effect, (ii) the strong deformation of the tetragonal axis with the N(2)−Mn−N(3) angle of about 30° below the expected value of 180°, and (iii) the deformation of the equatorial plane with the presence of the central nitrogen atom of bpea or terpy (N(1)).

Along the tetragonal axis, both the elongation and the angle are comparable for the three complexes: 4.492 Å < $d_{(Mn-N(2)+Mn-N(3))}$ < 4.524 Å; 149° < N(2)−Mn−N(3) < 151°. The nature of the ligand, bpea, or terpy has no effect on the N(2)−Mn−N(3) angle. On the contrary, slight effects can be noticed on the Mn−N(2) and Mn−N(3) bonds that are lengthened with bpea because of its flexible character, compared to that of terpy.

At this point, a correlation might be found between this previous analysis and the *D* parameter determined for each complex. In the case of pentacoordinated Mn(III) porphyrins or close derivatives such as corroles for which the spin Hamiltonian parameters were determined by HF-EPR spectroscopy, a C_{4v} point group, appropriate to describe the axial geometry of those complexes, was used.[9b] It was demonstrated that the spin−orbit coupling among the spin quintuplet states is not the unique factor which contributes to the magnitude of *D*. The energy separation between the spin ground state and the spin triplet excited state must also be taken into account. In our case, the distortions observed in the octahedron oblige us to use a D_{4h} symmetry as a first approximation. In this case, we can simply assume that *D* is inversely proportional to Δ_0, which is the energy separation between the ground state ($^5B_{1g}$ or $^5A_{1g}$, depending on the sign of *D*) and the ^5E_g state (ignoring the rhombic splitting). Accordingly, we should see a decrease of the magnitude of *D* when the azide ligands are replaced by the fluoride ligands, because fluoride anion is a stronger field ligand than azide anion. However, the contrary is observed (D(**3**) > D(**4**)), which establishes that another factor contributes to the magnitude of *D*. In this configuration, theoretical calculations must be performed to determine the orbital energy diagram of the quintuplet and triplet states of our complexes. This work is actually in progress and will give us supplementary information for the understanding of the *D* evolution as a function of the geometry of our complexes and of the contribution of the triplet state to *D*.

Regarding the deformation in the equatorial plane, correlation can be found between the degree of the plane deformation and the magnitude of the *E* term. The equatorial plane is more distorted in the fluoride complex (**3**) than in the azide complex (**4**) because the Mn−F bonds are shorter than the Mn−N_{azide} bonds and the Mn−N(1) bonds are longer than the Mn−N_X bonds (X = F^- or N_3^-). The length difference between the Mn−N(1) bond distance and the average distance of the Mn−X bonds for each complex is: **3**, 0.262 Å and **4**, 0.139 Å. This is in agreement with the *E* values: E(**3**) > E(**4**) (Table 4). A crystal field theory will be necessary to confirm this simple analysis since the *E* term is directly correlated with the spin−orbit coupling. Furthermore, calculations might define the hypothetical contribution of the spin excited state to the *E* value.

Concerning complex **2**, it cannot be compared to the other complexes because the geometry adopted around the Mn ion is different. Nevertheless, the magnitude of the *D* term (D = 3.50(1) cm^{-1}) is in the range limited by the other complexes (3.29 cm^{-1} < D < 3.82 cm^{-1}). As for the *E* term, it is clearly higher than for complexes **1**, **3**, and **4**. This is probably due to the N(2)−Mn−N(3) angle of 151.12°, which deforms drastically the equatorial plane.

Conclusion

In this study, we succeeded in synthesizing a new series of mononuclear Mn(III) complexes, two of them possessing Mn(III)−F bonds. The isolation and characterization of such compounds confirm that fluoride anions are able to coordinate strongly Mn(III). These results are consistent with the previous spectroscopic studies which suggest that fluoride anions inhibit the superoxide dismutase by binding to the Mn(III) site.[4]

The electronic properties of the complexes were determined accurately by a multifrequency EPR investigation, and some relations between their structural and electronic properties have been found. Nevertheless, theoretical calculations will be needed to confirm our analysis and to determine the contribution of the triplet state to the zero-field splitting parameters. This would consequently allow a complete characterization of their electronic properties and the correlation with the crystallographic structure.

The HF-EPR spectra of complex **1** obtained in solution display that a slight change of the structure occurs. This modification certainly takes place along the tetragonal axis

(18) (a) Griffith, J. S. *The Theory of Transition Metal Ions*; Cambridge University Press: New York, 1961. (b) Griffith, J. S. *Trans Faraday Soc*. **1960**, *56*, 193. (c) Abragam, A.; Bleaney, B. *Electron Paramagnetic Resonance of Transition Ions*; Oxford University Press: New York, 1970. (d) Bencini, A.; Ciofini, I.; Uytterhoeven, M. G. *Inorg. Chim. Acta* **1998**, *274*, 90.

(19) Gregson, A. K.; Doddrell, D. M.; Healy, P. C. *Inorg. Chem*. **1978**, *17*, 1216.

because the *D* term is the only spin Hamiltonian parameter modified. In addition, the absence of any broadening of the signal demonstrates that the structure is rigid in solution. This result makes the use of HF-EPR even more attractive, especially for proteins containing clusters whose characterization cannot be achieved by X-band EPR.

Acknowledgment. Fruitful discussions with Dr. G. Blondin from the University of Paris-Orsay, France, are acknowledged. We thank Dr. H. Weihe from the Chemistry Department, University of Copenhagen, Denmark, for the simulation software and Dr. J.-C. Leprêtre and C. Baffert, LEOPR, for their help in synthesis of the complexes.

Supporting Information Available: X-ray crystallographic details for complexes **1** (S1), **2** (S2), and **3** (S3) in CIF format. This material is available free of charge via the Internet at http://pubs.acs.org.

JA034652+